JGR Oceans

RESEARCH ARTICLE
10.1029/2020JC016898

Vertical Mixing in Stratified Fjords Near Tidewater Outlet Glaciers Along Northwest Greenland

Jørgen Bendtsen[1], Søren Rysgaard[2,3,4], Daniel F. Carlson[2,5,6], Lorenz Meire[4,7], and Mikael K. Sejr[2,8]

[1]Norwegian Institute for Water Research, NIVA Denmark, Copenhagen, Denmark, [2]Department of Biology, Arctic Research Center, Aarhus University, Aarhus, Denmark, [3]Center for Earth Observation Science, University of Manitoba, Winnipeg, MB, Canada, [4]Greenland Climate Research Center, Greenland Institute of Natural Resources, Nuuk, Greenland, [5]Department of Earth, Ocean, and Atmospheric Science, Florida State University, Tallahassee, FL, USA, [6]Now at Institute of Coastal Ocean Dynamics, Helmholtz-Zentrum Hereon, Geesthacht, Germany, [7]Department of Estuarine and Delta Systems, Royal Netherlands Institute for Sea Research, Yerseke, The Netherlands, [8]Department of Bioscience, Aarhus University, Silkeborg, Denmark

Key Points:

- Turbulence measurements in central parts of deep fjords in Northwest Greenland show weak turbulent vertical mixing in the upper 200 m
- Vertical mixing modified water masses in the inner part of fjords with tidewater outlet glaciers
- A vertical mixing hot spot in the upper ~100 m was observed in front of Store Gletscher

Supporting Information:

Supporting Information may be found in the online version of this article.

Correspondence to:

J. Bendtsen,
jb@niva-dk.dk

Citation:

Bendtsen, J., Rysgaard, S., Carlson, D. F., Meire, L., & Sejr, M. K. (2021). Vertical mixing in stratified fjords near tidewater outlet glaciers along Northwest Greenland. *Journal of Geophysical Research: Oceans*, *126*, e2020JC016898. https://doi.org/10.1029/2020JC016898

Received 16 OCT 2020
Accepted 15 JUL 2021

Abstract Vertical mixing of upper water masses in Arctic fjords is important for circulation and transport of nutrients and heat. However, the distribution of turbulent mixing is poorly known. Here we present hydrographic and microscale turbulence measurements from six fjords in Northwestern (69°N–75°N) Greenland. Water mass distributions showed the presence of warm bottom water of Atlantic origin in all fjord transects and a significant modification of upper water masses in fjords with tidewater outlet glaciers. Spatial and temporal distribution of turbulence in the fjords showed, in general, low rates of turbulent kinetic energy, ε (~10^{-9} W kg^{-1}), and strong stratification implies that vertical exchange in the upper ~200 m was relatively weak. However, measurements within 2 km of the terminus of a tidewater outlet glacier showed values of ε and inferred turbulent diffusion coefficients >10^{-4} m^2 s^{-1} that were about two orders of magnitude larger than elsewhere in the deep fjords. This elevated mixing corresponded to comparatively large heat and salt fluxes. These observations suggest that vertical mixing near tidewater outlet glaciers results in localized mixing hot spots, likely due to subglacial discharge and near-glacial current shear, that contribute significantly to vertical exchange in the deep fjords.

Plain Language Summary The Greenland Ice Sheet (GIS) is in direct contact with warm ocean water via glacier tongues that enter directly into fjords. Meltwater from the GIS and direct melt of glacial ice in the fjords generate dynamic areas near the glacier front with increased turbulence. Turbulent mixing brings warm and nutrient-rich water at depth up to the surface and, therefore, it is a key process influencing currents, submarine melting and biological productivity. However, we don't know how strong this vertical mixing is, since it has rarely been measured. We studied fjord systems in Northwestern Greenland, an area that is responsible for about a quarter of the current mass loss from GIS as either meltwater or solid ice. In general, mixing near the surface in these deep fjords was weak. However, mixing within about 2 km of a tidewater outlet glacier was about 100 times larger than elsewhere in the deep fjords. The turbulence measurements combined with profiles of temperature and salinity showed that vertical mixing from the small areas in front of tidewater outlet glaciers were mixing hot spots that bring heat and nutrients to the surface.

1. Introduction

Deep fjords around Greenland connect the Greenland ice sheet (GIS) and the ocean. The ice-ocean interaction takes place via tidewater outlet glaciers (TOGs), where the glaciers enter directly into the fjord (Straneo & Heimbach, 2013). From these marine terminating glaciers, buoyant freshwater released at depth gives rise to vigorous buoyant discharge plumes adjacent to the termini in the inner parts of the fjord. The water mass found down the fjord formed by mixing of buoyant subglacial freshwater and ambient fjord water and subsequent modification by glacial ice melt in the ice mélange is referred to as subglacial water (Mortensen et al., 2020). In addition, meltwater from land terminating glaciers (LTGs) is transported into the fjords at the surface via rivers. Runoff, meltwater from glacial ice and sea ice, and surface heating result in a relatively strong stratification in the upper part of the water column during the summer season. The stratified water

column tends to dampen vertical turbulent mixing and decreases associated fluxes of heat and salt. Weak mixing also limits the supply of nutrient-rich water to the surface layer and thereby biological production (e.g., Meire et al., 2017; Wassmann, 2011). In addition to the direct effects of vertical mixing on the physical and biological conditions, mixing also influences the circulation and exchange between the shelf and inner fjord through the modification of water masses and resulting horizontal pressure gradients (Mortensen et al., 2014, 2018).

Several fast-flowing TOGs enter directly into the ocean along Northwestern Greenland (Joughin et al., 2010) and ice-ocean interactions are, therefore, important there. Mass loss from the GIS has contributed to at least 2.5 cm of global-mean sea level rise during the twentieth century and currently the Northwestern GIS, that is, the relevant area for this study, accounts for ~25% of its total current mass loss (Kjeldsen et al., 2015).

Deep water masses are a major heat source for melting at the termini of TOGs (Christoffersen et al., 2011; Straneo et al., 2010). Relatively warm North Atlantic water masses have been identified as the cause for increased submarine melting along southeast Greenland (Holland et al., 2008; Straneo & Heimbach, 2013), and also impact glacier dynamics along western Greenland (e.g., Fenty et al., 2016; Mortensen et al., 2013; Rignot et al., 2016). Model simulations indicate that increased melt from subsurface heating could explain recent retreat of TOGs in Northwest Greenland (Wood et al., 2018).

Melting at the ice-ocean interface and mixing processes associated with subglacial discharge entrain ambient fjord water (Bendtsen, Mortensen, Lennert et al., 2015; Kimura et al., 2014; Motyka et al., 2003) and thereby increase near-glacial melting of glacial and sea ice (Mortensen et al., 2013), and may lead to increased calving (Chauché et al., 2014) when warm water masses are present. These processes are expected to enhance mixing rates near TOGs and, subsequently, enhance heat and nutrient fluxes and increase ecosystem productivity (Kanna et al., 2018; Meire et al., 2017), although vertical mixing is only one of several processes that impact primary production in fjord ecosystems (Hopwood et al., 2020). Other processes might drive vertical mixing in fjords, for example, mixing above shallow sills (e.g., Fer, 2006), narrow constrictions or localized fjord winds. Thus, vertical mixing is an important driver of physical and biogeochemical processes in deep fjord systems during the stratified summer season. However, few direct turbulence measurements have been made in Greenland fjords and the relative importance of mixing in the central parts of the fjords versus mixing near TOGs is poorly known.

Here we analyze water mass distributions and turbulent mixing in both TOG- and LTG-fjords in Northwestern Greenland during the stratified period in late summer. Water mass transformation is first related to mixing in front of TOGs and its imprint on upper water masses in the inner fjords is identified. We then analyze turbulence measurements from the entire area, including stations close to the terminus of a TOG. Finally, we discuss the impact of near-glacial mixing in TOG-fjords for nutrient transport and modification of upper water masses.

2. Methods

2.1. Study Area

Hydrographic and turbulence measurements were carried out on R/V Sanna in the period August 11–31, 2016 in six major fjord systems along Northwest Greenland from Kullorsuaq (~74.6°N) to Ataa Sound (~69.4°N, Figure 1a). The Northwest Greenland coastline is characterized by a high concentration of TOGs terminating in the fjords or, at locations without fjords, directly entering into the coastal water on the continental shelf (blue triangles, Figure 1a). TOGs were also present in four of the fjords investigated during the cruise (Kullorsuaq Fjord, Upernavik Icefjord, Uummannaq Fjord, and Ataa Sound). Two fjords with land-terminating glaciers were also investigated (Laksefjord, Greenlandic name: Eqalugaarsuit Sulluat, and Ukkusissat Fjord) and measurements were made close to the Rink outlet glacier in the Uummannaq Fjord system (the Uummannaq Fjord system encompass all fjords surrounding Uummannaq island, including Uummannaq Fjord). A single station was occupied in a southern branch of the Kullorsuaq Fjord system without TOGs. Measurements were made along the centerline of the fjords from the mouth and as close to the glacier termini as possible. Near-glacier turbulence measurements in the ice mélange in front of the terminus of Store Gletscher (Greenlandic name: Sermeq Kujalleq) in Uummannaq Fjord were made from

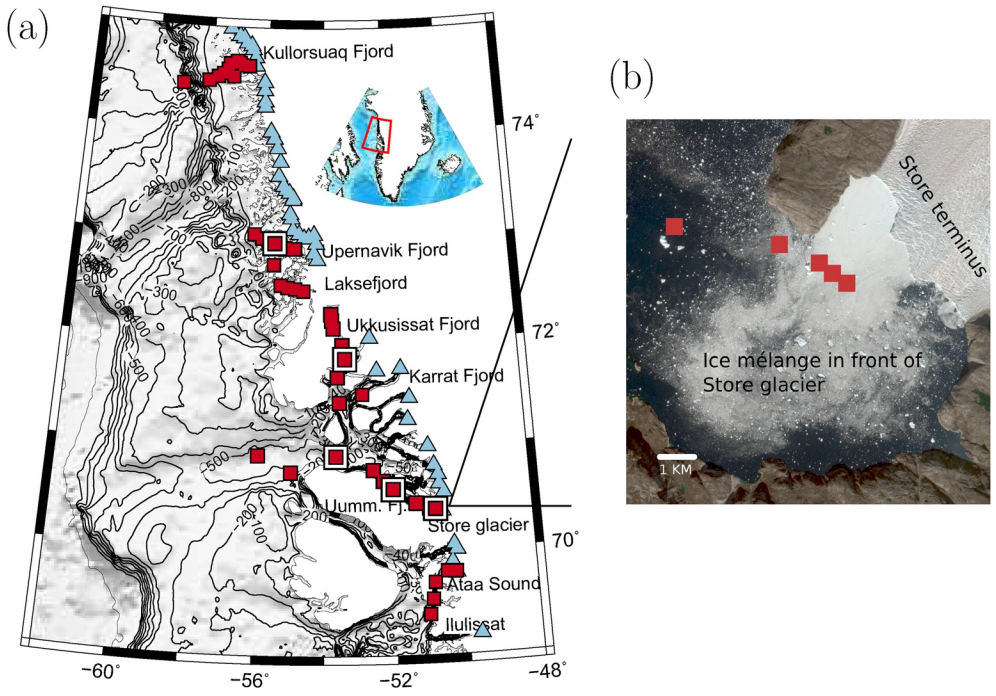

Figure 1. (a) Stations with conductivity, temperature and depth (CTD) and turbulence measurements (red squares), time series stations with turbulence measurements (white and red squares) and locations of tidewater outlet glaciers (TOGs) along Northwest Greenland (blue triangles). (b) Sentinel 2 image from August 16, 2016 of Store terminus and near-glacier stations with turbulence measurements (squares).

a small inflatable boat (Figure 1b). Two stations were located on the shelf off Kullorsuaq and Uummannaq Fjord.

The location of the termini from the outlet glaciers were estimated from Sentinel 2 satellite reflectance data obtained close to the sampling dates.

Bottom depths were measured along the fjord sections and bathymetry data from the Bedmachine data set (Morlighem et al., 2017) also supported the analysis.

2.2. Hydrographic and Turbulence Measurements

Conductivity, temperature and depth (CTD) measurements from surface to the bottom were carried out with a Seabird 19plus V2 CTD that was calibrated before the cruise. Salinities are reported on the TEOS-10 Absolute Salinity (S_A) scale (IOC et al., 2010). Salinity was significantly influenced by glacial runoff in the fjords, which may lead to deviations in the composition of dissolved salts in coastal water (e.g., Pawlowicz, 2015) compared with the open ocean water composition used in the calculation of S_A. Therefore, S_A was calculated assuming that the salinity anomaly (δS_A) was zero.

Microscale turbulence was measured with a loose-tethered, freely falling Rockland Scientific International (RSI) VMP-250 microstructure vertical profiler equipped with two shear probes, an FP07 thermistor, a microconductivity sensor and a conductivity, temperature (CT) and pressure-sensor (JFE Advantech, JAC). Microstructure measurements of shear, temperature and conductivity were sampled at 512 Hz, pressure was sampled at 64 Hz and the CT-sensor operated at 16 Hz.

Measurements obtained from the JAC-CTD and Seabird-CTD were compared by interpolating binned (0.5 dbar) JAC-CTD values onto the Seabird-CTD pressure between 170 and 185 dbar. The average difference (Seabird–JAC) between absolute salinity and potential temperature measurements were small (0.001 ± 0.017 g kg^{-1} and -0.014 ± 0.069°C, respectively, std. dev., $n = 609$) and the small deviations between the two instruments were considered negligible for the results presented here.

Turbulence profiles were obtained from the upper 200 m (sinking velocity ~0.6–0.7 m s^{-1}) from the free drifting ship (draught of 4.9 m) except for profiles made from a small inflatable dinghy near the terminus of Store Gletscher in Uummannaq Fjord. Profiles were obtained at 46 stations and typically two or more turbulence-profiler casts were made before the CTD at each station except for Kullorsuaq Fjord where only a single cast was made at each station. Repeated profiles to 200 m depth over extended time series were obtained at five stations (shown by white-outlined squares in Figure 1a): (a) Center of Upernavik Icefjord (72° 56.240′ N, 55° 37.897′ W, $n = 20$ profiles), (b) near the entrance to Ukkusissat Fjord (71° 50.088′ N, 53° 22.488′W, $n = 12$), (c) in the middle (I: 70° 35.239′ N, 51° 59.620′ W, $n = 10$) and (d) near the entrance of Uummannaq Fjord (II: 70° 54.366′N, 53° 39.794′ W, $n = 15$), and (e) at a distance of about 2 km from the terminus of Store Gletscher (~70° 22.668′N, 50° 39.740′ W, $n = 11$). Repeated profiles were conducted over periods of up to four hours at about the same location (except for measurements near the terminus at Store Gletscher and in Upernavik Icefjord where the station was moved due to moving drifting icebergs). A total of 154 microstructure profiles were made during the cruise.

2.3. Calculation of Turbulent Dissipation Rate, ε

The dissipation rate (ε) of turbulent kinetic energy (TKE) was calculated with software provided by Rockland Scientific (ODAS, ver. 4.0; Douglas & Lueck, 2015). Values of ε were estimated from below 5 m depth to reduce possible disturbances from the ship, and it was analyzed in bins of 8 s with 50% overlap, corresponding to a resolution of ~5 m (there were, in general, no clear indications of disturbances below 5 m, cf. Figures S2 and S3), following the method described by Wolk et al. (2002) and revised by Lueck (2016) (see Supporting Information S1).

Every cast provided two shear measurements and, in general, there was a relatively small deviation between the ε estimates from the two shear sensors. However, to remove outliers due to noise introduced during the operational procedure, the profiles were first inspected visually for spikes (identified from the horizontal accelerometer components) and segments of 10–40 m from five profiles were removed. Finally, a quality criteria of acceptable difference between the two shear sensors was defined (Bendtsen & Richardson, 2018) by analyzing data from time series station II in Uummannaq Fjord where the error distribution, defined from the difference of the logarithm ($\log_{10}$) between the two ε estimates (in W kg^{-1}), had an absolute standard deviation of 0.19 ($n = 803$). For measurements to be included in the analysis, the difference between the two sensors on the same profile should be less than 3 times the absolute deviation. This led to the removal of less than 4 per cent of the pairs of ε from the data set.

2.4. Calculation of k_v and Vertical Fluxes

The vertical turbulent diffusion coefficient (k_v) is calculated as $k_v = \Gamma\varepsilon/N^2$ (Osborn, 1980), where Γ is the mixing efficiency, N^2 is calculated from least squares linear fits to the density profile over intervals of 10 m as $N^2 = -g/\rho\ d\rho/dz$ with g being acceleration due to gravity, ρ is density and z is the vertical coordinate. Various parameterizations of the mixing efficiency have been evaluated and uncertainty and debate persist on this issue (Gregg et al., 2018). Here, we apply a parameterization that was suggested by Bouffard and Boegman (2013) based on a demonstrated relationship between the mixing efficiency and the turbulent mixing parameter (i.e., buoyancy Reynolds number) $Re_b = \varepsilon/\nu N^2$ This value is the ratio of the destabilizing influence from turbulence to the stabilizing effect from viscosity and stratification. The parameterization of k_v in terms of Re_b, that is, $k_v = \Gamma\nu Re_b$, implies a transitional regime (defined by Re_b) with a constant $\Gamma = 0.2$ and a decrease of Γ for low values of Re_b and when turbulence becomes energetic (i.e., $Re_b > 400$; Bouffard & Boegman, 2013; Shih et al., 2005; Table S1). A buoyancy-controlled regime characterizes mixing below the transitional regime and eventually mixing is determined by molecular diffusion for small values of Re_b (Table S1). Vertical fluxes of heat (F_H) and salinity (F_S) were calculated from k_v and the vertical gradient of the scalar fields, that is, $F_{H,S} = -k_v\ d\varphi/dz$, where φ is heat content (i.e., $\rho\ c_p\ \Theta$, in units of J m^{-3}, where c_p is the heat capacity for seawater) and salt content ($\rho\ S_A$, in units of $g\ m^{-3}$), respectively. The vertical gradient is calculated by linear regression of Θ and S_A over 10 m intervals.

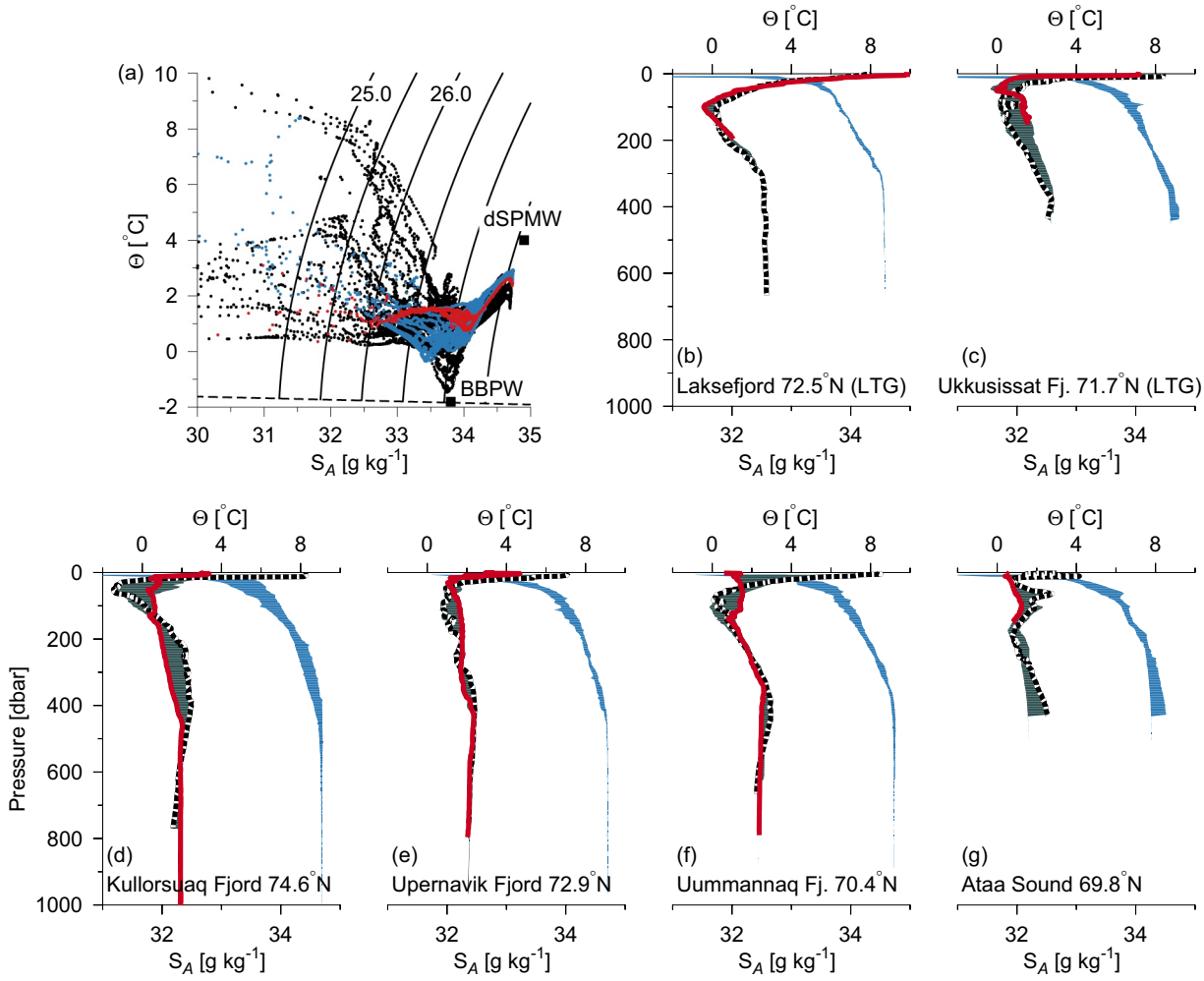

Figure 2. Conductivity, temperature and depth (CTD)-measurements from the study area. (a) Θ-S_A diagram of 0.5 m bin-averaged CTD-measurements where measurements in Uummannaq Fjord (blue) and in front of Store Gletscher (red) are indicated. Regional water masses are indicated and represented by deep Subpolar Mode Water (dSPMW, $\Theta \sim 4°C$, $S_A \sim 34.7$ g kg^{-1}) and Baffin Bay Polar Water (BBPW, $\Theta \sim -1.8°C$, $S_A \sim 33.6$ g kg^{-1}). (b–g) Selected profiles from six fjord systems where the total range of conservative temperature (dark gray) and absolute salinity (blue) are indicated. The nearest tidewater outlet glaciers (TOG)-profile, or profile near the head of the fjord, is shown in red and profiles at the fjord mouth are shown with white dashed lines. The two fjords with land-terminating glaciers are labeled as land terminating glaciers (LTG).

3. Results

3.1. Water Masses in Fjords Along Northwest Greenland

Subsurface distributions of Θ and S_A along eastern Baffin Bay can be related to two water masses originating from water types defined as Deep Subpolar Mode Water of Atlantic origin (dSPMW) observed on the slope and Baffin Bay Polar Water of Baffin Bay origin (BBPW, Rysgaard et al., 2020) in the upper ~150 m (Figure 2a). The presence of BBPW can, in general, be identified as a temperature minimum in the upper 100–150 m. Relatively warm ($\Theta \sim 2°C$) and salty ($S_A \sim 34.7$ g kg^{-1}) water shows the influence of dSPMW in the deeper parts of the fjords, whereas upper water masses varied significantly from the fjord mouth to the inner fjord (Figures 2b–2g). A clear temperature minimum in the upper 100 m (associated with BBPW) was seen in the inner part of the two fjords with a LTG (Figures 2b and 2c), whereas the temperature minimum from BBPW was absent in the inner part of fjords with TOGs (Figures 2d–2g).

An example of water mass modifications from the shelf toward a TOG is shown from the northernmost transect in Kullorsuaq Fjord, where the innermost station was 26 km from a major TOG (Figures 3a–3f). The fjord is relatively deep (>500 m) with a short transition zone from the entrance of the fjord to the water

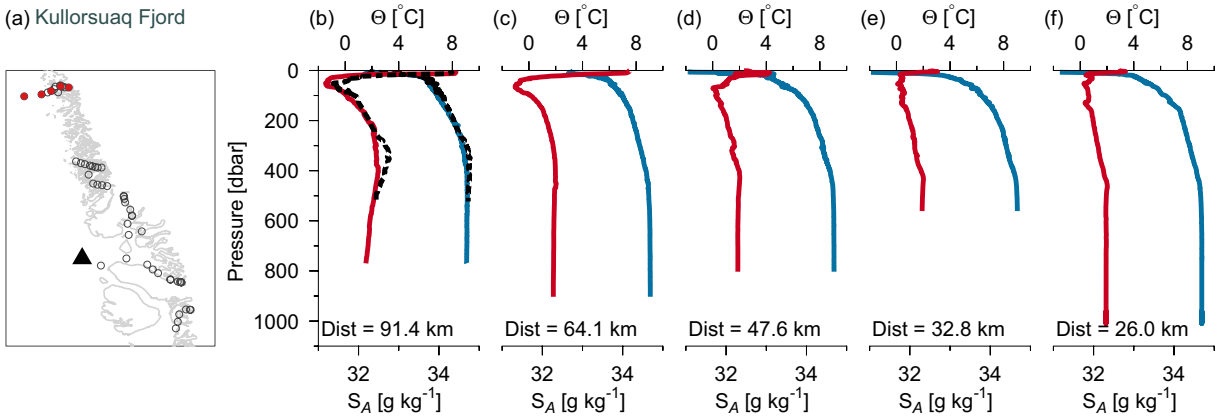

Figure 3. (a) Station map of selected stations along the northern transect in Kollorsuaq Fjord (red dots) and a single profile off Uummannaq Fjord (black triangle). Temperature (Θ, red) and salinity (S_A, blue) profiles (b–f) where the distance (Dist) to the tidewater outlet glaciers (TOG) is shown for each profile. Profiles of Θ and S_A are shown for the station off Uummannaq Fjord in (b) (dashed black lines).

masses at the slope, however, the detailed bathymetry of the fjord is poorly known. The relatively small difference in bottom water Θ-S_A characteristics between the fjord and the coastal station indicated a frequent or unhindered renewal of bottom water (Figure 2d). The temperature distribution outside the fjord at the westernmost station at the slope (Figure 3b) was characterized by BBPW in the upper 150 m and it was also seen as a temperature minimum in the upper 100 m inside and toward the middle of the fjord (in Figures 3c and 3d). The warmest (>2°C) subsurface water was observed outside the fjord (Figure 3b) where relatively warm dSPMW occupied the depth range between ~250 and 400 m (Θ = 2.48°C, see Table S2 for details of characteristics of Θ and S at selected stations). Relatively warm bottom water was present in the fjord below 400 m where temperatures were close to 2°C and a small temperature maximum below 400 m (mentioned above) could be traced all the way to the head of the fjord, as indicated by the innermost station off the glacier (Figures 3c–3f). A transition zone between inner fjord and coastal water masses was located in the middle of the fjord about 47.6 km from the TOG (near Figure 3d), where a relatively large horizontal temperature gradient characterized the depth range between 100 and 400 m depth. Similar transition zones were observed 49.7 km from the TOG in Upernavik Fjord (Figure S3i), 55.6 km from the TOG in Uummannaq Fjord (Figure S4j) and in the middle of Ukkusissat Fjord (Figure S4d).

Comparison between shelf and slope water masses off Kullorsuaq with the area off the Uummannaq Fjord further south (Figure 3a, triangle) showed that both areas were characterized by a well-defined temperature minimum at ~50–70 m depth associated with BBPW (Figure 3b, dashed line). The dSPMW was identified by a temperature maximum at ~370 m depth off Uummannaq Fjord and the warm water was also visible off Kullorsuaq, although it was more well-mixed in a thick sub-surface layer between 250 and 400 m depth. Thus, the water masses showed similar characteristics along this section of the Northwest Greenland shelf.

3.2. Influence From TOGs on Upper Water Masses

Two fjords, Ukkusissat Fjord and Uummannaq Fjord, were investigated in the Uummannaq Fjord system, representing fjords with an LTG and a TOG, respectively (Figure 4). The Uummannaq Fjord system contains several large TOGs and is connected to the broad shelf area through a deep (>500 m) trough from the outer slope (Figure 1a). The coastal station outside the Uummannaq Fjord system (hydrographic profiles shown in Figure 3b, dashed line) showed a clear maximum associated with dSPMW (maximum at 404 dbar, Θ = 2.98°C) above slightly colder water. The depth range of 50–120 m was characterized by BBPW with a clear temperature minimum (Θ = −0.91°C) and a relatively strong halocline toward the warm surface water (Θ = 7.88°C).

Ukkusissat Fjord is a deep, long and narrow fjord with an LTG at the head of the fjord (Figures 4a and 4c). The fjord was strongly stratified (Figure 4a) in the upper 100 m and a BBPW-temperature minimum was present at the innermost shallow station (Θ = −0.06°C, Table S2); this minimum was significantly colder

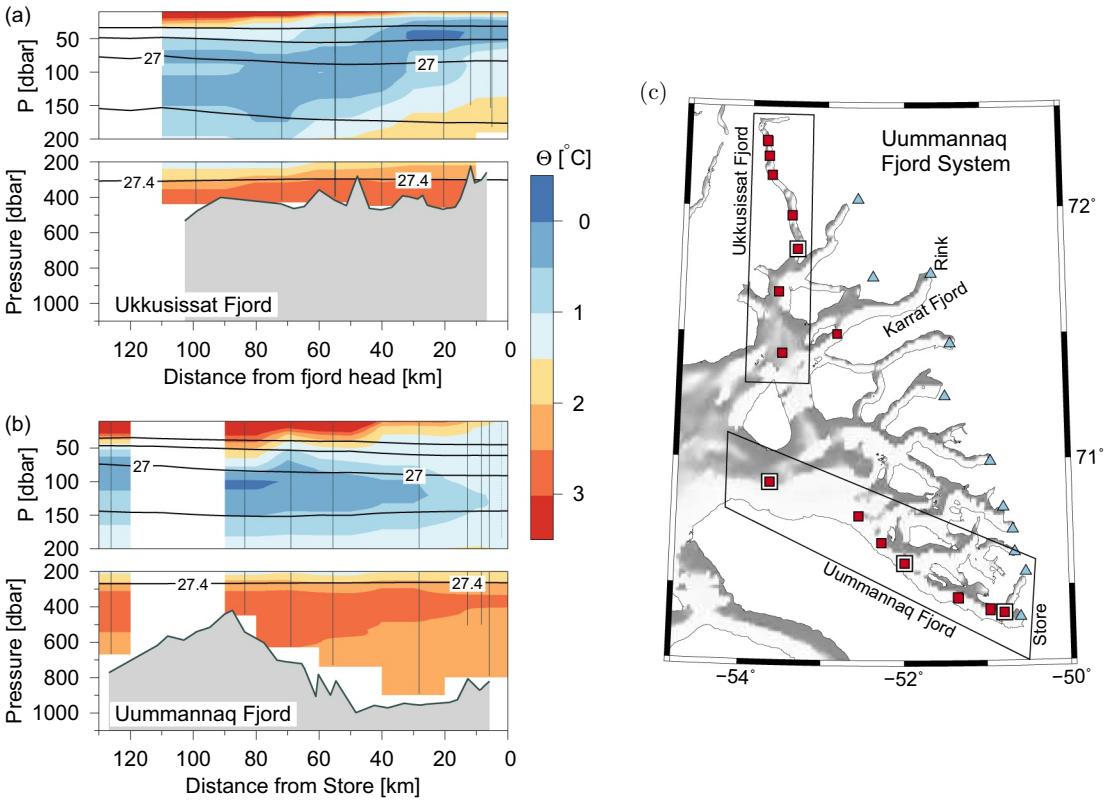

Figure 4. Transects of Θ (colors [°C]) versus the distance to the head of the fjord in (a) Ukkusissat Fjord and (b) Uummannaq Fjord, that is, the terminus of Store Gletscher is located to the right in (b). The upper figures show the upper 200 m with contour lines of potential density anomalies (σ^{Θ}) in intervals of 0.2 kg m^{-3}. (c) Station map of the Uummannaq fjord system with conductivity, temperature and depth (CTD) and turbulence measurements (red squares), time series stations with turbulence measurements (white and red squares) and locations of tidewater outlet glaciers (TOGs; blue triangles). Ukkusissat and Uummannaq fjord are indicated with rectangles.

than the surface water (Θ = ~6.8°C). The presence of a cold temperature minimum along the fjord was indicative of relatively weak vertical mixing in the upper 50–100 m.

Uummannaq Fjord is also part of the Uummannaq Fjord system and the main fjord branch terminates at a large TOG (Store Gletscher) with a smaller TOG (Lille Gletscher) in a neighboring fjord branch (Figures 4b and 4c). A distinct temperature minimum of BBPW was present at the entrance to the fjord and it gradually eroded toward the inner 20 km of the fjord where the innermost CTD-station only showed a weak temperature minimum.

In summary, the BBPW minimum could be traced to the innermost station in Ukkusissat Ford whereas it was eroded in Uummannaq Fjord, which implies that the dynamics and mixing of the upper sub-surface water masses differed markedly in these two adjacent fjords.

3.3. Turbulent Mixing and Temperature Minima

Turbulence and CTD (i.e., the JAC-CTD) measurements were collected down to ~200 m depth and profiles of Θ, S_A, ε and the vertical turbulent diffusion coefficient, k_v, are shown at selected stations along the six fjord sections in Figure 5, S3 and S4.

The upper water masses near the TOGs in Kullorsuaq Fjord were relatively warm (~0°C) and the station 19.8 km from the TOGs showed two clear temperature minima in the upper 50 m (Figure 5f). These two temperature minima are characteristic features associated with subglacial water near the terminus and their presence in the temperature profile about 20 km from the TOGs is indicative of advection of subglacially modified water (Mortensen et al., 2013, 2020). Values of ε were relatively weak ~10^{-9} W kg^{-1} and k_v

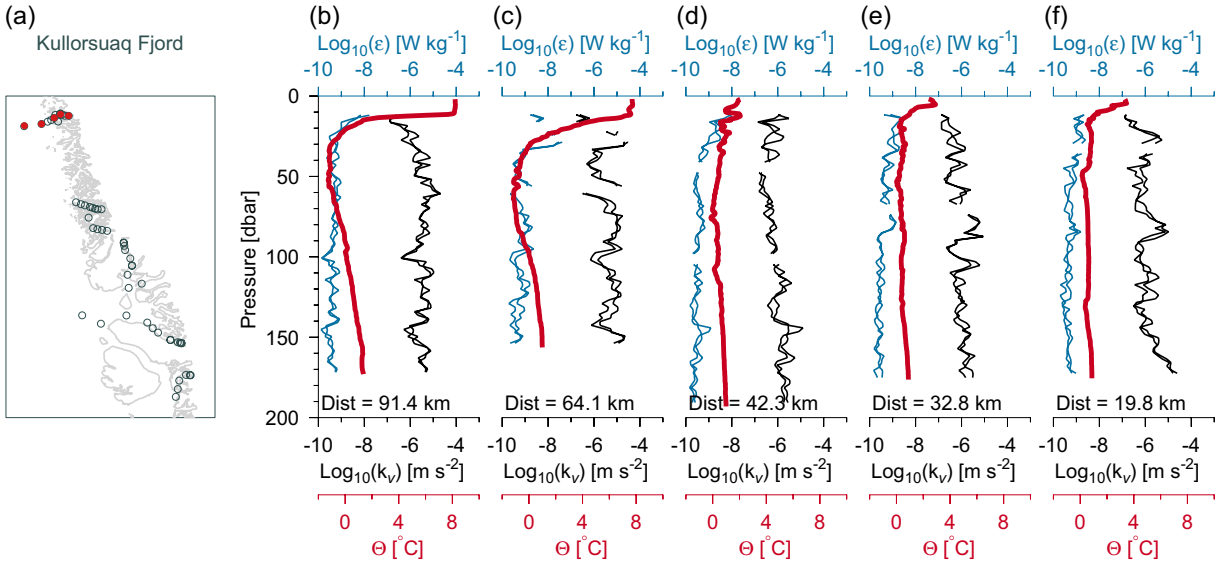

Figure 5. Station map and profiles of Θ (red) and the logarithm of ε (blue lines, W kg^{-1}) and k_v (black lines, m^2 s^{-1}) in Kullorsuaq Fjord (a–f). The abscissa covers both ε and k_v with their respective units and the two profiles represent estimates from each of the two shear probes.

was correspondingly small and in the range between 10^{-6} and 10^{-5} m^2 s^{-1}. Similar turbulence and CTD measurements were carried out along transects in the other five fjords (shown in Figures S3 and S4) and their distributions are summarized below.

Upernavik Icefjord (Figure S3g–S3l) is deep (~1,000 m) and the innermost station in the fjord was surrounded by 6–7 TOGs with dynamic subglacial discharge events (confirmed by satellite images, not shown) and iceberg calving. The temperature minimum of BBPW at the fjord entrance was present until the middle of the fjord (49.7–64.5 km from the TOGs) where the transition zone was associated with relatively large sub-surface vertical mixing at ~100 m depth ($k_v \sim 10^{-4}$ m^2 s^{-1}). Vertical mixing was relatively weak elsewhere in the fjord where k_v values of ~10^{-5} m^2 s^{-1} below 100 m depth decreased to ~10^{-6} m^2 s^{-1} toward the surface layer.

Laksefjord (Figure S3m–S3q), located ~50 km south of Upernavik Icefjord, is a relatively deep fjord (~600 m depth) that is, surrounded by LTGs. The stratified water column with a clear temperature minimum of BBPW showed that this LTG-fjord was characterized by a relatively weak vertical mixing of subsurface water in accordance with the low ε and k_v values of ~10^{-9} W kg^{-1} and <10^{-5} m^2 s^{-1}, respectively.

The station off the Ukkusissat Fjord mouth (Figures 4a and S4b) showed relatively large vertical mixing in the upper 100 m ($k_v > 10^{-5}$–10^{-4} m^2 s^{-1}) and mixing in this dynamical area, toward the outflow from Rink Gletcher (the terminus in Karrat Fjord, Figure 4c) may explain the absence of a BBPW-temperature minimum in the outer part of the fjord. A clear temperature minimum was present at the innermost stations and these stations were also characterized by relatively low mixing rates ($\varepsilon < 10^{-9}$ W kg^{-1}, $k_v \sim 10^{-6}$–10^{-5} m^2 s^{-1}). The temperature minimum was an indication of residing BBPW from the winter season. Thus, low vertical mixing characterized the inner part of this LTG-fjord during the summer season.

The station off the Uummannaq Fjord mouth (Figure S4h) showed a relatively high sub-surface mixing below ~60 m corresponding to the situation off Ukkusissat Fjord. Vertical mixing was relatively low in the fjord, whereas relatively high vertical mixing rates were observed in front of the terminus of Store Gletscher in the end of the fjord (Figure S4l, $k_v \sim 10^{-3}$ m^2 s^{-1}).

Ataa Sound connects to Disko Bay via a shallow 150–200 m sill (Rignot et al., 2016). A subsurface temperature maximum beneath the surface layer (Θ = 2.78°C) and a temperature minimum at ~190 m depth (Θ = 0.76°C) characterized the upper water column (Figures S4m–S4r; Table S2). The presence of a warmer upper water mass showed that conditions in Disko Bay differed significantly from conditions further north on the shelf. The upper temperature extremum was partly eroded at the innermost station (Figure S4r),

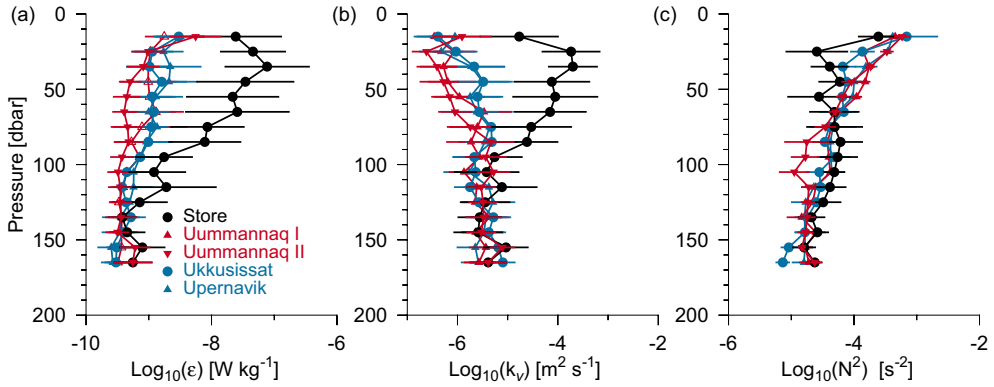

Figure 6. Vertical profiles of binned geometric averages (a) ε, (b) k_v, and (c) N^2 from 5 time series. Error bars show the geometric standard deviation (standard factor).

where the depth is only 81 m and relatively warm water (>2°C) was present below 200 m depth in the central part of the fjord. Elevated mixing was observed below ~80 m depth about ~3 km from the terminus (not shown, $k_v \sim 10^{-4}$ m^2 s^{-1}). With this exception, the fjord was characterized by relatively low vertical mixing ($k_v < 10^{-5}$ m^2 s^{-1}).

In summary, the fjords were characterized by low vertical mixing except near a TOG. In the two fjords with only LTGs a clear temperature minimum of BBPW was present in the entire fjord section whereas the BBPW temperature minimum was eroded toward the TOGs.

3.4. Time Series of Turbulence Profiles

Time series of turbulence profiles in the upper 200 m from the central and outer part of the three fjords showed general low values of ε (Figure 6). Average values of ε are in the range 1–5 × 10^{-9} W kg^{-1} in the upper 50 m and values below 10^{-9} W kg^{-1} characterized the profiles below. Strong stratification in the upper 50 m due to the seasonal halocline and thermocline ($N^2 \sim 10^{-4}$ s^{-2}) resulted in a k_v in the range 10^{-6}–10^{-5} m^2 s^{-1}. These low values imply weak vertical mixing in the upper 50 m. The average value of k_v below 50 m remained below 10^{-5} m^2 s^{-1}. Time series of turbulence profiles at four locations about 2 km away from the terminus of Store Gletscher in the ice mélange (Figure 1b) revealed values of ε in the upper 100 m that were 1–2 orders of magnitude larger than observed in the other time series (Figure 6a). Also, the temporal variability was significantly larger, showing that the area in front of the terminus was more dynamic and associated with significantly larger turbulence. The stratification was weaker in the upper 50 m (Figure 6c) in accordance with the increased turbulent mixing. Vertical diffusion coefficients were also 1–2 orders of magnitude larger in the upper 100 m than values obtained at the other time series stations (Figure 6b).

3.5. Vertical Distribution of Vertical Mixing in the Fjords

Distributions of ε and k_v were analyzed in four depth intervals (5–20 m; 20–50 m; 50–100 m; 100–200 m) and in four groups representing; (a) conditions in front of the terminus of Store Gletscher, (b) in Uummannaq Fjord (except profiles included in group I), (c) Ukkusissat Fjord, and (d) all the remaining data grouped in "Other stations" (Figure 7). Conditions in the fjords were characterized by relatively low vertical mixing (k_v generally less than 10^{-5} m^2 s^{-1}) except for the area in front of Store Gletscher where ε and k_v were about two orders of magnitude larger in the upper 100 m. For example, the geometric average of ε ($\overline{\varepsilon}$) and k_v ($\overline{k_v}$) in the depth range between 20 and 50 m depth in front of Store Gletscher were $5.0{\cdot}10^{-8}$ W kg^{-1} ranging within $1.0{\cdot}10^{-8}$ – $2.4{\cdot}10^{-7}$ W kg^{-1} (interval based on the geometric standard deviation) and $1.4{\cdot}10^{-4}$ m^2 s^{-1} ($3.1{\cdot}10^{-5}$–$6.5{\cdot}10^{-4}$ m^2 s^{-1}), respectively. The corresponding values of $\overline{\varepsilon}$ and $\overline{k_v}$ in the remaining part of Uummannaq Fjord in the same depth interval were characterized by relatively low values of $1.2{\cdot}10^{-9}$ W kg^{-1} ($4.1{\cdot}10^{-10}$–$3.5{\cdot}10^{-9}$ W kg^{-1}) and $9.4{\cdot}10^{-7}$ m^2 s^{-1} ($1.8{\cdot}10^{-7}$–$5.0{\cdot}10^{-6}$ m^2 s^{-1}), respectively. Low values also characterized profiles obtained at the other stations in the upper 100 m. Thus, vertical turbulent mixing was, in

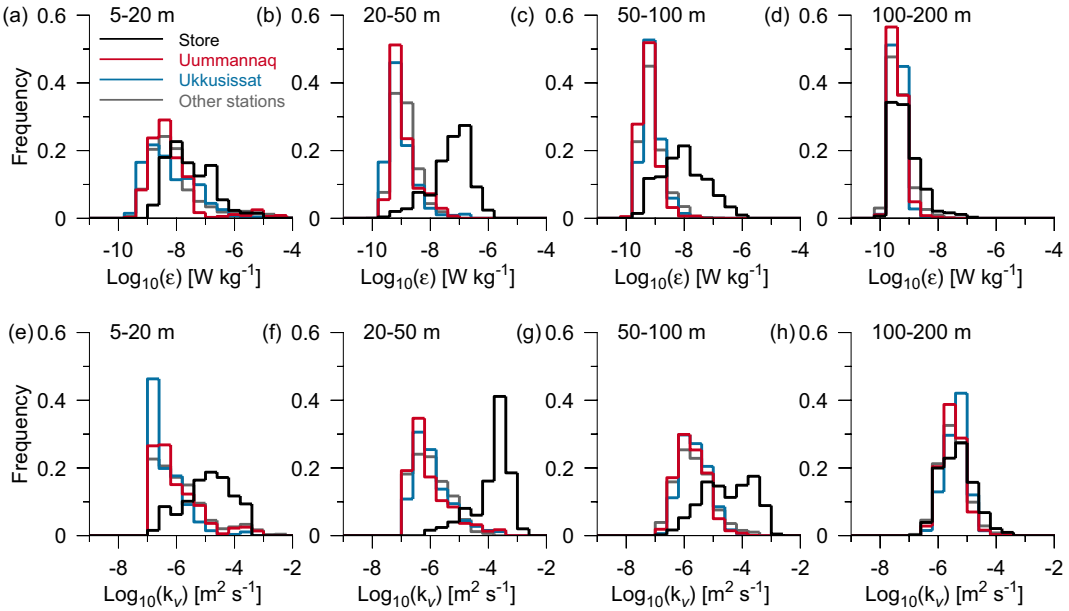

Figure 7. Distributions of $\log_{10}(\varepsilon)$ (upper panels) and $\log_{10}(k_v)$ (lower panels) in depth ranges between (a and e) 5–20 m, (b and f) 20–50 m, (c and g) 50–100 m and (d and h) 100–200 m.

general, 1–2 orders of magnitude larger in the upper 100 m in front of the terminus of Store Gletscher than at other stations in the study area.

3.6. Mixing in Front of Store Gletscher Terminus

We hypothesize that elevated vertical mixing in front of the glacier is due to energetic flow associated with subglacial discharge plumes or melting glacier ice. Therefore, the nearest 6 turbulence-profiles obtained from three stations closest to Store Gletscher (Figure 1b) were examined in detail. The turbulence profiles were compared with two profiles from the CTD station located ~6.3 km from the terminus (the western-most red square in Figure 1b) made before and after the turbulence profiles (~3 h) and relatively small temporal variation showed that no major subsurface changes were taking place during this period (Figure 8). The depth averaged salinity flux in front of the terminus in the depth range between 20 and 50 m was

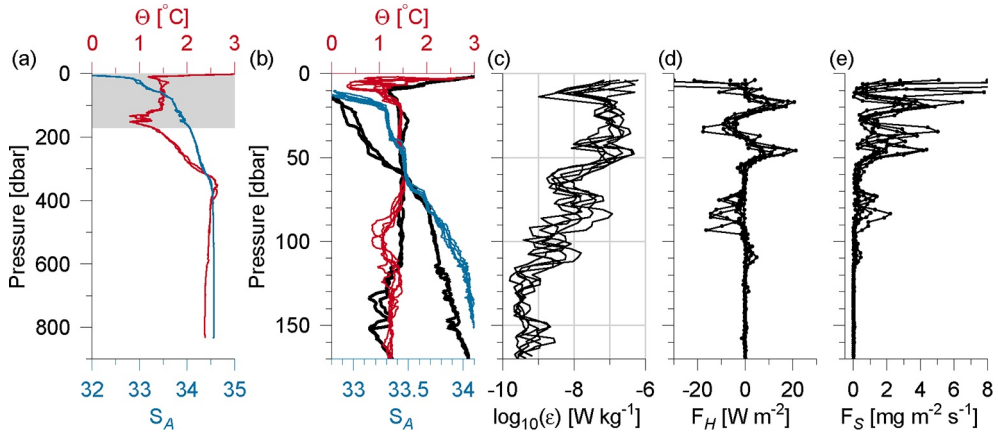

Figure 8. (a) Conductivity, temperature and depth (CTD)-profiles of Θ (red) and S_A (blue) near Store Gletscher made before and after the near-terminus turbulence profiles were made (lightgray box shows the depth range in b–e). (b) Θ (red) and S_A (blue) profiles near Store Gletscher. CTD-profiles from (a) are shown in black. (c) $\log_{10}(\varepsilon)$, (d) heat-flux and (e) salinity-flux.

$1.3 \pm 1.1 \cdot 10^{-3}$ g m^{-2} s^{-1} (std. dev., $n = 208$) and this was two orders of magnitude larger than the average from the rest of the fjord ($0.06 \pm 0.14 \cdot 10^{-3}$ g m^{-2} s^{-1}, $n = 372$). Similarly, on average, the heat flux in the same depth range was positive in front of the glacier (0.6 ± 0.4 W m^{-2}, $n = 208$), whereas a mean heat flux, associated with a relatively large standard deviation, of -0.20 ± 1.6 W m^{-2} ($n = 372$) characterized the rest of the fjord.

Water masses in front of the terminus are influenced by subglacial discharge and associated entrainment of bottom water during summer (Bendtsen, Mortensen, Lennert et al., 2015), and this explains the observed background level of high salinity and relatively high temperatures in the upper 100–150 m compared with ambient water further from the TOG. Elevated vertical mixing was observed in a depth range of up to 100 m in front of the terminus and may likely be due to disturbances induced by intruding sub-surface plume water originating from subglacial discharge or meltwater from the terminus.

4. Discussion

4.1. Weak Vertical Mixing in Deep Fjords

Bottom water in fjords along Northwest Greenland was dominated by relatively warm dSPMW below ~300 m and was separated from the surface layer by a cold layer of BBPW in the upper 150 m, in accordance with previous observations from the area (e.g., Fenty et al., 2016; Rignot et al., 2016; Rysgaard et al., 2020). In general, weak vertical mixing was found to characterize the upper 200 m in the fjords except for locations close to TOGs. Thus, weak vertical turbulent mixing is likely representative for conditions in the stratified summer period where wind, waves and baroclinic eddies are damped by the narrow fjords that are often surrounded, and protected from wind, by steep mountain topography. Note, however, that the measurements were carried out in relatively calm weather. For example, short katabatic wind events are occasionally observed in fjords around Greenland and, although they typically occur outside the summer season (e.g., Oltmanns et al., 2014), they may have a significant influence on vertical mixing in the fjords. Benthic boundary layers in fjords have been found to be up to several hundred meters thick (Kunze et al., 2012) and larger mixing rates have also been found in shallower Arctic fjords (Fer & Widell, 2007). However, fjords along Northwest Greenland are typically deep (~500–1,000 m) and upper water masses are therefore only marginally influenced by the bottom boundary layer.

The relatively low estimates of ε, with typical values between 10^{-10} and 10^{-9} W kg^{-1} (the noise floor is about 10^{-10} W kg^{-1}, see SI) in the central parts of the fjords, were comparable with conditions in other Arctic areas, for example, with open ocean values from the Arctic Ocean (Rippeth et al., 2015), the Beaufort Sea area (Scheifele et al., 2018) and correspondingly weak vertical nitrate fluxes have been observed across the Arctic (Randelhoff et al., 2020). The low observed values of ε in this study and the relatively strong stratification during this time of the year implied k_v values typically between 10^{-6} and 10^{-5} m^2 s^{-1} in the upper 200 m. Thus, these values indicate that vertical turbulent mixing in fjords in NW Greenland is very small and has a negligible impact on fluxes of heat, salt, and nutrients. Tidal amplitudes are modest (0.5–1 m) along the Northwestern coast (Padman & Erofeeva, 2004) compared with tides south of Davis Strait (Richter et al., 2011), however, vertical mixing, and associated fluxes, may be locally enhanced by strong tidal flows over topographic features like sills (e.g., Mortensen et al., 2011), at junctions between fjord branches, and through constrictions.

4.2. Mixing Hot Spots Near Tidewater Outlet Glaciers

Estimates of ε and k_v were about 1–2 orders of magnitude larger within about 2 km of the terminus than elsewhere in the fjords, supporting our conclusion that areas in front of TOGs can be considered as mixing hot spots. Previous studies have shown observations of sub-surface currents several kilometers from the terminus associated with subglacial discharge events (Jackson et al., 2017; Mankoff et al., 2016; Slater et al., 2018) and the associated vertical current shear may provide energy for turbulent mixing. Laboratory experiments also indicate increased vertical mixing associated with subduction of plume water (Cenedese & Gatto, 2016). Model studies support that vertical mixing influences the upper water masses in front of the termini of TOGs (e.g., Bendtsen, Mortensen & Rysgaard, 2015; Sciascia et al., 2013; Slater et al., 2018) and the distribution of tracers also indicates enhanced mixing (Beaird et al., 2015).

We observed relatively deep and elevated vertical mixing about 2 km from the TOG and in periods without visible subglacial discharge plumes. We cannot rule out, however, that subglacial plumes occurred that could not be seen from the surface in our small boat. Other sources of mixing may also be at play, for example, mixing from iceberg motion. A general relatively deep and elevated mixing domain in front of the TOGs would have a major influence on heat, salt and nutrient transports in addition to mixing directly associated with subglacial discharge plumes.

Vertical mixing in front of Store Gletscher suggest that TOGs can play a similar key role as sills or topographic constrictions as hot spots for vertical exchange in the deep stratified fjords. Furthermore, mixing near TOGs implies that mixing occurs in a relatively deep upper layer covering a depth range of up to ~100 m. In addition to the high values of ε and k_v, the salinity flux was also found to be ~2 orders of magnitude larger in front of the terminus than further down-fjord, and heat fluxes were found to be positive in the upper 50 m, contrary to the remaining part of the fjord. This implies that the area-integrated impact from these diffusive fluxes may be comparable to mixing integrated over ~100 km of the low-energetic fjord section. Thus, high vertical mixing rates in a small area in front of the glaciers may have a disproportionately large influence on vertical exchange in the upper ~100 m in the TOG fjords.

4.3. Transition Zone Between Inner- and Outer Water Masses

Mortensen et al. (2020) showed that melting of glacial ice in the ice mélange down-fjord from a subglacial discharge plume in Godthåbsfjord (64°N) resulted in a water mass, referred to as subglacial water, localized between two temperature minima. Our measurements showed a similar subglacial water signal in the inner part of TOG fjords that could be traced ~50 km down-fjord, whereas this was absent in LTG fjords. The down-fjord location of the front between inner and outer water masses can be explained either as a semi-permanent feature where supply from subglacial discharge and subsequent formation of subglacial water is balanced by mixing with outer water masses in the frontal zone, or as a gradual advection of subglacial water from the TOG toward the fjord mouth during the summer season. Further measurements are necessary for a more complete description of this process. However, previous studies have shown that transport of nutrient-rich bottom water associated with subglacial discharge explains high biological production in TOG fjords (Meire et al., 2017), and also that transport of nutrient-rich subglacial water gives rise to increased production downstream of a TOG (Meire et al., 2016). Similarly, high production may therefore characterize the outflowing subglacial water toward these frontal zones in the fjords.

5. Conclusion

Deep fjords along Northwest Greenland in late summer shared several common features, and conditions in the upper 200 m could furthermore be characterized in terms of fjords either having a tidewater outlet glacier (TOG) or a land-terminating glacier (LTG). The presence of relatively warm ($\Theta \sim 2$°C) and salty ($S_A \sim 34.7$ g kg^{-1}) bottom water below 300 m showed the influence of deep subpolar mode water (dSPMW, deep Subpolar Mode Water) of Atlantic origin in all the fjords visited between 69.8°N and 74.6°N, and this confirmed that warm water of Atlantic origin was present as bottom water in deep fjords along this section of the coast A distinct temperature minimum (<0°C), associated with BBPW (Baffin Bay Polar Water), was also present at ~50–70 m depth on the shelf, and this temperature minimum was observed to the inner part of the two fjords with a LTG. In the inner part of fjords with TOGs the temperature minimum was eroded, which we explain as a response to elevated mixing observed in front of the TOGs. A time series of turbulence ~2 km from the terminus of Store Gletscher supports this interpretation: at this location, dissipation rates of turbulent kinetic energy and estimates of the vertical turbulent diffusion coefficient here were 1–2 orders of magnitude larger in the upper 100 m than at stations further from the TOGs. These observations have two important implications: (a) vertical mixing in the fjords was, in general, relatively weak in the upper 200 m whereas (b) observations in front of Store Gletscher suggest that increased mixing close to TOGs takes place in a relatively deep layer (~100 m) and in a distance of 1–2 km from the terminus and thereby may contribute significantly to vertical exchange in fjords with TOGs. The transition from outer- to inner-fjord water masses modified by TOGs occurred typically ~50 km from the terminus. Elevated and deep vertical mixing in a relatively large area (1–2 km) in front of TOGs may, therefore, act as a localized mixing hot spot and, together with other mixing areas such as in subglacial discharge plumes and shallow

sills and topographic narrowing of the fjord width, these hot spots drive significant vertical transports of heat, salt, nutrients and other dissolved substances toward the surface layer.

Data Availability Statement

Bathymetric data referred to in the analysis was obtained from Morlighem et al. (2017), updated 2018. IceBridge BedMachine Greenland, Version 3. Boulder, Colorado USA. NASA National Snow and Ice Data Center Distributed Active Archive Center (https://doi.org/10.5067/2CIX82HUV88Y, accessed September 9, 2019). Copernicus Sentinel data 2019, for Sentinel data. CTD-data from the Sanna cruise are archived at ICES (https://ices.dk) and at Zenodo (http://doi.org/10.5281/zenodo.4062024), and turbulence measurements are also archived at Zenodo (http://doi.org/10.5281/zenodo.4090228).

Acknowledgments
The Danish Center for Marine Research is acknowledged for funding ship time. We also acknowledge the contributions of the Canada Excellence Research Chair (CERC) program, support provided by the Natural Sciences and Engineering Research (NSERC) Council, the Canada Foundation for Innovation, the University of Manitoba and Aarhus University. The Carlsberg foundation provided support for the turbulence instrument (CF15-0301). The captain and crew on R/V Sanna are acknowledged for their excellent assistance on board. Mikael K. Sejr received funding from the EU Horizon2020 project INTAROS. Lorenz Meire was funded by research programme VENI (016.Veni.192.150, NWO). This work is a contribution to the ArcticNet Networks of Centers of Excellence and the Arctic Science Partnership (ASP, asp-net.org).

References

Beaird, N., Straneo, F., & Jenkins, W. (2015). Spreading of Greenland meltwaters in the ocean revealed by noble gases. *Geophysical Research Letters*, *42*, 7705–7713. https://doi.org/10.1002/2015GL065003

Bendtsen, J., Mortensen, J., Lennert, K., & Rysgaard, S. (2015). Heat sources for glacial ice melt in a West Greenland tidewater outlet glacier fjord: The role of subglacial freshwater discharge. *Geophysical Research Letters*, *42*, 4089–4095. https://doi.org/10.1002/2015GL063846

Bendtsen, J., Mortensen, J., & Rysgaard, S. (2015). Modelling subglacial discharge and its influence on ocean heat transport in Arctic fjords. *Ocean Dynamics*, *65*, 1535–1546. https://doi.org/10.1007/s10236-015-0883-1

Bendtsen, J., & Richardson, K. (2018). Turbulence measurements suggest high rates of new production over the shelf edge in the north-eastern North Sea during summer. *Biogeosciences*, *15*, 7315–7332. https://doi.org/10.5194/bg-15-7315-2018

Bouffard, D., & Boegman, L. (2013). A diapycnal diffusivity model for stratified environmental flows. *Dynamics of Atmospheres and Oceans*, *61–62*, 14–34. https://doi.org/10.1016/j.dynatmoce.2013.02.002

Cenedese, C., & Gatto, V. M. (2016). Impact of a localized source of subglacial discharge on the heat flux and submarine melting of a tidewater glacier: A laboratory study. *Journal of Physical Oceanography*, *46*, 3155–3163. https://doi.org/10.1175/JPO-D-16-0123.1

Chauché, N., Hubbard, A., Gascard, J.-C., Box, J. E., Bates, R., Koppes, M., et al. (2014). Ice–ocean interaction and calving front morphology at two west Greenland tidewater outlet glaciers. *The Cryosphere*, *8*, 1457–1468. https://doi.org/10.5194/tc-8-1457-2014

Christoffersen, P., Mugford, R. I., Heywood, K. J., Joughin, I., Dowdeswell, J. A., Syvitski, J. P. M., et al. (2011). Warming of waters in an East Greenland fjord prior to glacier retreat: Mechanisms and connection to large-scale atmospheric conditions. *The Cryosphere*, *5*, 701–714. https://doi.org/10.5194/tc-5-701-2011

Douglas, W., & Lueck, R. (2015). *Library, Technical manual version 4.0. Rockland scientific international* (p. 155). Canada.

Fenty, I., Willis, J. K., Khazendar, A., Dinardo, S., Forsberg, R., Fukumori, I., et al. (2016). Oceans melting Greenland: Early results from NASA's ocean-ice mission in Greenland. *Oceanography*, *29*, 72–83. https://doi.org/10.5670/oceanog.2016.100

Fer, I. (2006). Scaling turbulent dissipation in an Arctic fjord. *Deep Sea Research Part II: Topical Studies in Oceanography*, *53*, 77–95. https://doi.org/10.1016/j.dsr2.2006.01.003

Fer, I., & Widell, K. (2007). Early spring turbulent mixing in an ice-covered Arctic fjord during transition to melting. *Continental Shelf Research*, *27*, 1980–1999. https://doi.org/10.1016/j.csr.2007.04.003

Gregg, M. C., D'Asaro, E. A., Riley, J. J., & Kunze, E. (2018). Mixing efficiency in the ocean. *Annual Review of Marine Science*, *10*, 443–473. https://doi.org/10.1146/annurev-marine-121916-063643

Holland, D., Thomas, R. H., de Young, B., Ribergaard, M., & Lyberth, B. (2008). Acceleration of Jakobshavn Isbræ triggered by warm subsurface ocean waters. *Nature Geoscience*, *1*, 659–664. https://doi.org/10.1038/ngeo316

Hopwood, M. J., Carroll, D., Dunse, T., Hodson, A., Holding, J. M., Iriarte, J. L., et al. (2020). How does glacier discharge affect marine biogeochemistry and primary production in the Arctic? *The Cryosphere*, *14*, 1347–1383. https://doi.org/10.5194/tc-14-1347-2020

IOC, SCOR & IAPSO. (2010). The international thermodynamic equation of seawater–2010: Calculation and use of thermodynamic properties. Intergovernmental Oceanographic Commission, Manuals and Guides No. 56, UNESCO (English), 196pp.

Jackson, R. H., Shroyer, E. L., Nash, J. D., Sutherland, D. A., Carroll, D., Fried, M. J., et al. (2017). Near-glacier surveying of a subglacial discharge plume: Implications for plume parameterizations. *Geophysical Research Letters*, *44*, 6886–6894. https://doi.org/10.1002/2017GL073602

Joughin, I., Smith, B. E., Howat, I. M., Scambos, T., & Moon, T. (2010). Greenland flow variability from ice-sheet-wide velocity mapping. *Journal of Glaciology*, *56*, 415–430. https://doi.org/10.3189/002214310792447734

Kanna, N., Sugiyama, S., Ohashi, Y., Sakakibara, D., Fukamachi, Y., & Nomura, D. (2018). Upwelling of macronutrients and dissolved inorganic carbon by a subglacial freshwater driven plume in Bowdoin Fjord, northwestern Greenland. *Journal of Geophysical Research: Biogeosciences*, *123*, 1666–1682. https://doi.org/10.1029/2017JG004248

Kimura, S., Holland, P. R., Jenkins, A., & Piggott, M. (2014). The effect of meltwater plumes on the melting of a vertical glacier face. *Journal of Physical Oceanography*, *44*, 3099–3117. https://doi.org/10.1175/JPO-D-13-0219.1

Kjeldsen, K. K., Korsgaard, N. J., Bjørk, A. A., Khan, S. A., Box, J. E., Funder, S., et al. (2015). Spatial and temporal distribution of mass loss from the Greenland Ice Sheet since AD 1900. *Nature*, *528*, 396–400. https://doi.org/10.1038/nature16183

Kunze, E., MacKay, C., McPhee-Shaw, E. E., Morrice, K., Girton, J. B., & Terker, S. R. (2012). Turbulent mixing and exchange with interior waters on sloping boundaries. *Journal of Physical Oceanography*, *42*, 910–927. https://doi.org/10.1175/JPO-D-11-075.1

Lueck, R. (2016). Calculating the rate of dissipation of turbulent kinetic energy (RSI Technical Note 028). In: *Rockland Scientific International* (p. 18). Canada.

Mankoff, K. D., Straneo, F., Cenedese, C., Das, S. B., Richards, C. G., & Singh, H. (2016). Structure and dynamics of a subglacial discharge plume in a Greenlandic fjord. *Journal of Geophysical Research: Oceans*, *121*, 8670–8688. https://doi.org/10.1002/2016JC011764

Meire, L., Mortensen, J., Meire, P., Juul-Pedersen, T., Sejr, M., Rysgaard, S., et al. (2017). Marine-terminating glaciers sustain high productivity in Greenland fjords. *Global Change Biology*, *23*, 1–5357. https://doi.org/10.1111/gcb.13801

Meire, L., Mortensen, J., Rysgaard, S., Bendtsen, J., Boone, W., Meire, P., & Meysman, F. J. R. (2016). Spring bloom dynamics in a subarctic fjord influenced by tidewater outlet glaciers (Godthåbsfjord, SW Greenland). *Journal of Geophysical Research: Biogeosciences*, *121*, 1581–1592. https://doi.org/10.1002/2015jg003240

Morlighem, M., Williams, C. N., Rignot, E., An, L., Arndt, J. E., Bamber, J. L., et al. (2017). BedMachine v3: Complete bed topography and ocean bathymetry mapping of Greenland from multibeam echo sounding combined with mass conservation. *Geophysical Research Letters*, *44*, 11051–11061. https://doi.org/10.1002/2017GL074954

Mortensen, J., Bendtsen, J., Lennert, K., & Rysgaard, S. (2014). Seasonal variability of the circulation system in a west Greenland tidewater outlet glacier fjord, Godthåbsfjord (64°N). *Journal of Geophysical Research: Earth Surface*, *119*, 2591–2603. https://doi.org/10.1002/2014jf003267

Mortensen, J., Bendtsen, J., Motyka, R. J., Lennert, K., Truffer, M., Fahnestock, M., & Rysgaard, S. (2013). On the seasonal freshwater stratification in the proximity of fast-flowing tidewater outlet glaciers in a sub-Arctic sill fjord. *Journal of Geophysical Research: Ocean*, *118*, 1–1395. https://doi.org/10.1002/jgrc.20134

Mortensen, J., Lennert, K., Bendtsen, J., & Rysgaard, S. (2011). Heat sources for glacial melt in a sub-Arctic fjord (Godthåbsfjord) in contact with the Greenland Ice Sheet. *Journal of Geophysical Research*, *116*, C01013. https://doi.org/10.1029/2010JC006528

Mortensen, J., Rysgaard, S., Arendt, K. E., Juul-Pedersen, T., Søgaard, D. H., Bendtsen, J., & Meire, L. (2018). Local coastal water masses control heat levels in a West Greenland tidewater outlet glacier fjord. *Journal of Geophysical Research: Oceans*, *123*, 8068–8083. https://doi.org/10.1029/2018JC014549

Mortensen, J., Rysgaard, S., Bendtsen, J., Lennert, K., Kanzow, T., Lund, H., & Meire, L. (2020). Subglacial discharge and its down-fjord transformation in West Greenland fjords with an ice mélange. *Journal of Geophysical Research: Oceans*, *125*, e2020JC016301. https://doi.org/10.1029/2020JC016301

Motyka, R. J., Hunter, L., Echelmeyer, K. A., & Connor, C. (2003). Submarine melting at the terminus of a temperate tidewater glacier, LeConte Glacier, Alaska, USA. *Annals of Glaciology*, *36*, 57–65. https://doi.org/10.3189/172756403781816374

Oltmanns, M., Straneo, F., Moore, G. W. K., & Mernild, S. H. (2014). Strong downslope wind events in Ammassalik, Southeast Greenland. *Journal of Climate*, *27*, 977–993. https://doi.org/10.1175/jcli-d-13-00067.1

Osborn, T. R. (1980). Estimate of the local rate of vertical diffusion from dissipation measurements. *Journal of Physical Oceanogaphy*, *10*, 83–89. https://doi.org/10.1175/1520-0485(1980)010<0083:eotlro>2.0.co;2

Padman, L., & Erofeeva, S. (2004). A barotropic inverse tidal model for the Arctic Ocean. *Geophysical Research Letters*, *31*, LO2303. https://doi.org/10.1029/2003GL019003

Pawlowicz, R. (2015). The absolute salinity of seawater diluted by riverwater. *Deep-Sea Research*, *101*, 71–79. https://doi.org/10.1016/j.dsr.2015.03.006

Randelhoff, A., Holding, J., Janout, M., Sejr, M. K., Babin, M., Tremblay, J. É., & Alkire, M. B. (2020). Pan-Arctic Ocean primary production constrained by turbulent nitrate fluxes. *Frontiers in Marine Science*, *7*, 150. https://doi.org/10.3389/fmars.2020.00150

Richter, A., Rysgaard, S., Dietrich, R., Mortensen, J., & Petersen, D. (2011). Coastal tides in West Greenland derived from tide gauge records. *Ocean Dynamics*, *61*, 39–49. https://doi.org/10.1007/s10236-010-0341-z

Rignot, E., Fenty, I., Xu, Y., Cai, C., Velicogna, I., Cofaigh, C. Ó., et al. (2016). Bathymetry data reveal glaciers vulnerable to ice-ocean interaction in Uummannaq and Vaigat glacial fjords, west Greenland. *Geophysical Research Letters*, *43*, 2667–2674. https://doi.org/10.1002/2016GL067832

Rippeth, T. P., Lincoln, B. J., Lenn, Y. D., Green, J. M., Sundfjord, A., & Bacon, S. (2015). Tide-mediated warming of Arctic halocline by Atlantic heat fluxes over rough topography. *Nature Geoscience*, *8*, 191–194. https://doi.org/10.1038/ngeo2350

Rysgaard, S., Boone, W., Carlson, D., Sejr, M. K., Bendtsen, J., Juul-Pedersen, T., et al. (2020). An updated view on water masses on the pan-West Greenland continental shelf and their link to proglacial fjords. *Journal of Geophysical Research: Oceans*, *125*, e2019JC015564. https://doi.org/10.1029/2019jc015564

Scheifele, B., Waterman, S., Merckelbach, L., & Carpenter, J. R. (2018). Measuring the dissipation rate of turbulent kinetic energy in strongly stratified, low-energy environments: A case study from the Arctic Ocean. *Journal of Geophysical Research: Oceans*, *123*, 5459–5480. https://doi.org/10.1029/2017JC013731

Sciascia, R., Straneo, F., Cenedese, C., & Heimbach, P. (2013). Seasonal variability of submarine melt rate and circulation in an East Greenland fjord. *Journal of Geophysical Research: Oceans*, *118*, 2492–2506. https://doi.org/10.1002/jgrc.20142

Shih, L. H., Koseff, J. R., Ivey, G. N., & Ferziger, J. H. (2005). Parameterization of turbulent fluxes and scales using homogeneous sheared stably stratified turbulence simulations. *Journal of Fluid Mechanics*, *525*, 193–214. https://doi.org/10.1017/S0022112004002587

Slater, D. A., Straneo, F., Das, S. B., Richards, C. G., Wagner, T. J. W., & Nienow, P. W. (2018). Localized plumes drive front-wide ocean melting of a Greenlandic tidewater-glacier. *Geophysical Research Letters*, *45*, 12350–12358. https://doi.org/10.1029/2018GL080763

Straneo, F., Hamilton, G. S., Sutherland, D. A., Stearns, L. A., Davidson, F., Hammill, M. O., et al. (2010). Rapid circulation of warm subtropical waters in a major glacial fjord in East Greenland. *Nature Geoscience*, *3*, 182–186. https://doi.org/10.1038/ngeo764

Straneo, F., & Heimbach, P. (2013). North Atlantic warming and the retreat of Greenland's outlet glaciers. *Nature*, *504*, 36–43. https://doi.org/10.1038/nature12854

Wassmann, P. (2011). Arctic marine ecosystems in an era of rapid climate change. *Progress in Oceanography*, *90*, 1–17. https://doi.org/10.1016/j.pocean.2011.02.002

Wolk, F., Yamazaki, H., Seuront, L., & Lueck, R. G. (2002). A new free-fall profiler for measuring bio-physical microstructure. *Journal of Atmosphere and Ocean Technology*, *19*, 780–793. https://doi.org/10.1175/1520-0426(2002)019<0780:anffpf>2.0.co;2

Wood, M., Rignot, E., Fenty, I., Menemenlis, D., Millan, R., Morlighem, M., et al. (2018). Ocean-induced melt triggers glacier retreat in Northwest Greenland. *Geophysical Research Letters*, *45*, 8334–8342. https://doi.org/10.1029/2018GL078024

References From the Supporting Information

Caldwell, D. (1974). Thermal conductivity of sea water. *Deep-Sea Research and Oceanographic Abstracts*, *21*, 131–137. https://doi.org/10.1016/0011-7471(74)90070-9

Chen, C. T., & Millero, F. J. (1977). Speed of sound in seawater at high pressures. *Journal of the Acoustical Society of America*, *62*, 1129–1135. https://doi.org/10.1121/1.381646

Feistel, R. (2003). A new extended Gibbs thermodynamic potential of seawater. *Progress in Oceanography*, *58*, 43–114. https://doi.org/10.1016/s0079-6611(03)00088-0

Fer, I., Peterson, A. K., & Ullgren, J. E. (2014). Microstructure measurements from an underwater glider in the turbulent Faroe Bank Channel Overflow. *Journal of Atmospheric and Oceanic Technology*, *31*(5), 1128–1150. https://doi.org/10.1175/jtech-d-13-00221.1

Jackson, P. R., & Rehmann, C. R. (2014). Experiments on differential scalar mixing in turbulence in a sheared, stratified flow. *Journal of Physical Oceanography*, *44*, 2661–2680. https://doi.org/10.1175/JPO-D-14-0027.1

Sharqawy, M. H., Lienhard, J. H., & Zubair, S. M. (2010). The thermophysical properties of seawater: A review of existing correlations and data. *Desalination and Water Treatment*, *16*, 354–380. https://doi.org/10.5004/dwt.2010.1079

Sun, H., Feistel, R., Koch, M., & Markoe, A. (2008). New equations for density, entropy, heat capacity, and potential temperature of a saline thermal fluid. *Deep-Sea Research I*, *55*, 1304–1310. https://doi.org/10.1016/j.dsr.2008.05.011